Cholesterol crystallization within hepatocyte lipid droplets and its role in murine NASH

George N. Ioannou,[1,*,†] Savitha Subramanian,[§] Alan Chait,[§] W. Geoffrey Haigh,[*] Matthew M. Yeh,[**] Geoffrey C. Farrell,[††] Sum P. Lee,[†] and Christopher Savard[*,†]

Division of Gastroenterology, Department of Medicine,* Veterans Affairs Puget Sound Health Care System, Seattle, WA; Division of Gastroenterology,[†] Division of Metabolism, Endocrinology and Nutrition,[§] and Department of Pathology,** University of Washington, Seattle, WA; and Liver Research Group,[††] Australian National University Medical School at the Canberra Hospital, Garran, ACT, Australia

Abstract **We recently reported that cholesterol crystals form in hepatocyte lipid droplets (LDs) in human and experimental nonalcoholic steatohepatitis. Herein, we assigned WT C57BL/6J mice to a high-fat (15%) diet for 6 months, supplemented with 0%, 0.25%, 0.5%, 0.75%, or 1% dietary cholesterol. Increasing dietary cholesterol led to cholesterol loading of the liver, but not of adipose tissue, resulting in fibrosing steatohepatitis at a dietary cholesterol concentration of ⩾0.5%, whereas mice on lower-cholesterol diets developed only simple steatosis. Hepatic cholesterol crystals and crown-like structures also developed at a dietary cholesterol concentration ⩾0.5%. Crown-like structures consisted of activated Kupffer cells (KCs) staining positive for NLRP3 and activated caspase 1, which surrounded and processed cholesterol crystal-containing remnant LDs of dead hepatocytes. The KCs processed LDs at the center of crown-like structures in the extracellular space by lysosomal enzymes, ultimately transforming into lipid-laden foam cells. When HepG2 cells were exposed to LDL cholesterol, they developed cholesterol crystals in LD membranes, which caused activation of THP1 cells (macrophages) grown in coculture; upregulation of *TNF-alpha*, *NLRP3*, and interleukin 1beta (*IL1β*) mRNA; and secretion of IL-1beta. In conclusion, cholesterol crystals form on the LD membrane of hepatocytes and cause activation and cholesterol loading of KCs that surround and process these LDs by lysosomal enzymes.—** Ioannou, G. N., S. Subramanian, A. Chait, W. G. Haigh, M. M. Yeh, G. C. Farrell, S. P. Lee, and C. Savard. **Cholesterol crystallization within hepatocyte lipid droplets and its role in murine NASH. *J. Lipid Res.* 2017.** 58: **1067–1079.**

Supplementary key words cholesterol crystal • nonalcoholic steatohepatitis • lipotoxicity • fatty liver

The histological hallmark of nonalcoholic fatty liver disease (NAFLD) is increased lipid deposition within lipid droplets (LDs) in hepatocytes, a process known as hepatic steatosis. In the majority of patients, hepatic steatosis occurs in the absence of concomitant inflammation or fibrosis. This "simple steatosis" carries a very low risk of progression to cirrhosis or liver dysfunction (1). However, a small subset of patients with NAFLD (10%–30%) develop a more aggressive condition known as nonalcoholic steatohepatitis (NASH), which can progress to cirrhosis (1, 2) and is characterized by hepatocellular injury (e.g., manifesting as ballooning of hepatocytes) and varying degrees of hepatic inflammation and fibrosis, in addition to hepatic steatosis.

The factor (or factors) responsible for the development of progressive NASH, as opposed to simple steatosis, remains unclear. Recent studies suggest that cholesterol is an important lipotoxic molecule that promotes the development of NASH in many, diverse animal models (3–12). Human epidemiological studies (13) and clinical trials of cholesterol-lowering drugs (14–20) appear to also support a role of cholesterol in the development of NASH. The mechanisms by which cholesterol might exert lipotoxicity and promote the development of NASH remain unclear (21). We recently reported that cholesterol crystals developed within the LDs of steatotic hepatocytes in patients with NASH and in a mouse model of NASH induced by a high-fat, high-cholesterol (HFHC) diet, but not in patients or mice with simple steatosis (22). We also demonstrated that enlarged Kupffer cells (KC) surrounded steatotic, dead hepatocytes containing cholesterol crystals and appeared to process the remnant LDs within these hepatocytes, forming "crown-like structures" (CLS) similar to those previously described in inflamed visceral adipose tissue (23, 24). Cholesterol crystals have recently been

This work was supported by the Diabetes Research Center, University of Washington (G.N.I.), and by the Veterans Affairs Biomedical and Laboratory Research and Development Grant I01BX002910 (G.N.I.). No conflicts of interest exist.

Manuscript received 3 October 2016 and in revised form 3 April 2017.

Published, JLR Papers in Press, April 12, 2017
DOI https://doi.org/10.1194/jlr.M072454

Abbreviations: CLS, crown-like structure; HFHC diet, high-fat, high-cholesterol diet; KC, Kupffer cell; LD, lipid droplet; LDL-C, LDL cholesterol; NAFLD, nonalcoholic fatty liver disease; NASH, nonalcoholic steatohepatitis.

[1] To whom correspondence should be addressed.
e-mail: georgei@medicine.washington.edu

The online version of this article (available at http://www.jlr.org) contains a supplement.

shown to activate the NLRP3 inflammasome in animal models of atherosclerosis (25, 26), thus providing a mechanism by which exposure of KC to cholesterol crystals can lead to chronic inflammation and NASH. Treatment with ezetimibe and atorvastatin led to resolution of cholesterol crystals and CLSs together with amelioration of NASH (27).

In the present study we aimed to further characterize the development and implications of hepatic cholesterol crystallization in vivo and to develop an in vitro cell culture model of steatosis and cholesterol crystallization.

MATERIALS AND METHODS

Animal procedures

Four-month-old, male C57BL/6J, WT, littermate mice (Jackson Laboratory, Bar Harbor, ME) were assigned to a high-fat (15%, weight/weight) diet for 6 months, supplemented with 0%, 0.25%, 0.5%, 0.75%, or 1% dietary cholesterol (five groups; n = 12 mice/group). Cocoa butter, which contains approximately 60% saturated fat, was the source of the extra fat in these diets (22, 27). Their composition is shown in supplemental Table S1. Mice were housed four per cage with unrestricted access to food and water. Mice were euthanized 6 months after initiation of the experimental diets by cervical dislocation following isoflurane anesthesia. All experimental procedures were approved by the Institutional Animal Care and Use Committee of the Veterans Affairs Puget Sound Health Care System.

Histological assessment of steatosis, inflammation, and fibrosis

Formalin-fixed, paraffin-embedded liver tissue sections were stained with H&E, Masson's trichrome, or Sirius red (for collagen). Histological steatosis, inflammation, and fibrosis were assessed semiquantitatively with the scoring system of Kleiner et al. (28) by a "blinded," expert hepatopathologist (M.M.Y.). Sirius red-stained collagen fibers were also quantified by using a polarizing microscope with digital image analysis (National Institutes of Health Image J density software), as the average of 10 random 200× fields without major blood vessels (6). Immunohistochemical staining for α-smooth muscle actin was performed as a marker of stellate cell activation.

Assessment of hepatic cholesterol crystals and free cholesterol

Liver pieces were embedded in OCT compound and frozen in liquid nitrogen immediately after harvest. Frozen sections (10 μM in thickness) were allowed to come to room temperature, immediately cover-slipped with glycerol as the mounting medium without applying any stain, and examined using a Nikon Eclipse microscope with or without a polarizing filter, to evaluate for the presence of birefringent cholesterol crystals, as we previously reported (22, 27). Frozen liver sections were stained with filipin, which identifies free cholesterol by interacting with its 3β-hydroxy group to fluoresce blue (29).

To better distinguish LDs with or without cholesterol crystals, we used a special method of osmium tetroxide fixation and staining, followed by methylene blue counterstaining, which we recently described (22). Small pieces (~2 mm^2) of liver tissue previously fixed in Trump's fixative were submerged in 1% osmium tetroxide for 1 h on ice, frozen in OCT, cut into 5-μm sections, and counterstained with 0.05% methylene blue. Osmium tetroxide binds at the carbon-carbon double bonds of unsaturated fatty acid chains in triglycerides and cholesterol esters and therefore nicely distinguishes the free-cholesterol crystals, which do not stain with osmium, from the triglyceride and cholesterol esters within LDs, which stain gray-black.

Identification of activated KCs and CLSs

Frozen liver sections were stained with anti-CLEC4F antibody (R&D Systems Inc., Minneapolis, MN), which identifies resident macrophages/KCs, and with anti-Ly6c (Thermo Fisher Scientific, Fremont, CA), which identifies recruited myeloid cells, to confirm that CLSs comprised resident macrophages/KCs as opposed to recruited myeloid cells. Frozen liver sections were also stained with anti-CD68 and anti-F4/80 antibodies, which identify macrophages (including hepatic KCs) and with anti-TNF-α antibodies, which identify *activated* M1 macrophages as we have previously described (22, 27). CLS can be readily identified by TNF-α staining as rings of activated KCs surrounding and processing steatotic hepatocytes containing cholesterol crystals. The number of CLSs that stained with anti-TNF-α in 10 random 200× fields (area = 0.14 mm^2/field) per liver was averaged. Acid phosphatase staining was used to identify the lysosomes of KCs within CLSs.

Evidence of NLRP3 activation

We stained liver sections with anti-NLRP3 antibodies to look for expression of this component of the NLRP3 inflammasome in the KCs of CLSs, as we have previously described (27). Liver sections were also stained for activated (cleaved) caspase 1, using the FAM-FLICA caspase 1 assay kit (27). We used real-time PCR (RT-PCR) to quantify mRNA gene expression levels, as previously described (7), of the following components of the NLRP3 inflammasome in liver tissue: *Caspase-1*, *Nalp3*, and apoptosis-associated speck-like, caspase recruitment domain-containing protein (*Asc*) (30).

Hepatic lipid analysis

Lipids were extracted from frozen mouse liver by using the Folch method (31). The neutral lipid fractions were prepared by solid phase extraction, and the triglycerides, cholesterol esters, and free cholesterol were then separated and quantified by normal-phase HPLC/Evaporative Light Scattering Detector (ELSD).

Other measurements

Hepatic gene expression levels were measured by RT-PCR for chemotactic factors (monocyte chemoattractant protein-1 [*Mcp1*]) and proinflammatory factors (serum amyloid A1 [*Saa1*], Egf-like module-containing, mucin-like, hormone receptor-like 1 [*Emr1* or *F4/80*], interleukin-1b [*Il1b*], and *Tnfa*). Blood specimens were collected immediately prior to sacrifice after a 4-h fast and tested for plasma cholesterol, triglycerides, alanine aminotransferase (ALT), glucose, and insulin. Food consumption was measured and averaged weekly.

Cell culture

HepG2 cells plated in 24-well culture plates (or 2-well glass chamber slides) were cultured in basal medium with 10% fetal bovine serum and 2 mg/ml of the ACAT inhibitor Sandoz 58-035 (Sigma Chemical, St. Louis, MO) to inhibit esterification of cholesterol and hence increase free cholesterol and cholesterol crystallization until confluent (~1.5 million cells/well); they were then supplemented for 20 days (twice/week) with *a*) control media; *b*) 200 mg/dl of LDL cholesterol (LDL) (human plasma LDL; Lee Biosystems, Maryland Heights, MO); *c*) 200 μM of oleic acid (OA) (Thermo Fisher Scientific, Asheville, NC); or *d*) both

LDL (200 mg/dl) and OA (200 μM). At the end of this 20-day period, THP-1 cells, differentiated into macrophages by a 2-day treatment with 20–40 nM of PMA (32, 33), were directly cocultured with the HepG2 cells for 3 h (for mRNA expression studies) or for 24 h (for protein expression studies), after washing the HepG2 cells with regular media to remove any residual LDL or oleic acid. PMA-activated THP-1 macrophages have been shown to produce pro-IL-1beta and to secrete IL-1beta in response to direct exposure to cholesterol crystals in a dose-dependent manner (26). Cell culture systems were stained with Sudan black (fat) and were evaluated for cholesterol crystallization by polarized light microscopy and filipin staining and by NLRP3 activation by mRNA assays of NLRP3 components and protein studies for secreted IL-1β in the supernatants.

In additional experiments, PMA-treated THP-1 cells were grown on Transwell® inserts (0.4-μm pore size); then the inserts were suspended above the HepG2 cells that had been treated with control or LDL or with OA, as was described above. Media from the top and bottom of the insert were collected at 24 h, and IL-1beta was measured by ELISA.

RESULTS

Fibrosing NASH develops at a threshold dietary cholesterol concentration of 0.5% in WT C57BL/6 mice

Increasing dietary cholesterol concentration from 0% to 1% caused increasing liver weight and liver weight: body weight ratio (**Table 1**). This was caused primarily by an increase in hepatic cholesterol ester concentration, though hepatic triglyceride concentration did not increase. Plasma ALT (a marker of hepatic necroinflammation) and plasma cholesterol levels increased with increasing dietary cholesterol.

Although severe histological hepatic steatosis (grade 3) was evident with all dietary cholesterol concentrations, substantial hepatic histological inflammation and fibrosis, indicative of NASH, occurred only at a dietary cholesterol at or above 0.5% (Table 1 and **Fig. 1**). Quantitative Sirius red staining confirmed the abrupt rise in hepatic fibrosis at a threshold dietary cholesterol of 0.5%.

Although increasing dietary cholesterol composition from 0% to 1% led to a 60-fold increase in hepatic cholesterol ester content, it did not lead to any increase in the cholesterol ester content of subcutaneous or epididymal fat. Thus excess dietary cholesterol seems to be stored in the liver rather than in adipose tissue.

Analysis of mRNA transcripts showed that dietary cholesterol increased the expression of chemotactic (*Mcp1*) and proinflammatory (*Saa1*, *F4/80*, *Il1b*, and *Tnfα*) genes and genes related to the NLRP3 inflammasome (*Caspase 1*, *Nlrp3*, and *Asc*) (supplemental Fig. S1). Interestingly, maximum expression occurred with 0.75% dietary cholesterol rather than 1% cholesterol.

Hepatocyte cholesterol crystals and crown-like structures of activated KCs also develop at a threshold dietary cholesterol concentration of 0.5%

Substantial cholesterol crystallization developed within hepatocyte LDs at the same threshold dietary cholesterol concentration (at or above 0.5%) that induced fibrosing NASH (Table 2 and Fig. 1). Filipin staining confirmed that the crystalline birefringent material within hepatocyte LDs was free cholesterol (**Fig. 2**). Activated TNF-α-positive KCs (Fig. 2), which were also positive for CD68, F4/80, and CLEC4F but negative for Ly6C (supplemental Fig. S2), surrounded the most intensely birefringent LDs forming characteristic CLSs, which also became evident at a threshold dietary cholesterol concentration of ⩾0.5%.

Characterization of cholesterol crystallization

In intact hepatocytes that were not surrounded by CLS, cholesterol crystallization was evident in the periphery of their large LDs in association with the LD membrane (**Fig. 3A**, B). However, in the remnant LDs of dead hepatocytes that were surrounded and processed by KC in a CLS, the entire LD contained crystallized cholesterol (Fig. 3C, D). LDs that were entirely birefringent as in Fig. 3C, D were always in the middle of a CLS. This suggests that additional free cholesterol is formed after the hydrolysis of cholesterol esters by the lysosomal enzymes of the surrounding KCs, leading to more dramatic cholesterol crystallization.

Characterization of crown-like structures and NLRP3 activation

At high magnification, CLSs are shown to consist of multiple KCs and other macrophages that surround large-remnant LDs of dead hepatocytes containing multiple cholesterol crystals (Fig. 3C, D). The KCs that make up CLSs appear to be in direct apposition to each other, surrounding and enclosing the remnant LD and directly abutting it without any intervening hepatocyte cytoplasm or cell membrane (supplemental Fig. S3), thus demonstrating that the hepatocyte is dead. KCs processing remnant LDs of hepatocytes were transformed into characteristic foam cells containing multiple small LDs (Fig. 3E, F). Also these KCs in CLSs strongly express acid phosphatase (Fig. 3J), suggesting that lysosomal enzymes are released into the LD in the center of the CLS to hydrolyze its triglyceride and cholesterol ester content. In addition to TNF-α, the KCs in CLSs are shown by immunohistochemistry to express Nlrp3 (Fig. 3G) and activated caspase 1 (Fig. 3I). The presence of cleaved caspase 1 confirms activation of the inflammasome pathway in KCs within CLS as a possible response to cholesterol crystals in NASH.

THP-1 cells cocultured with HepG2 cells induced to develop large LDs and cholesterol crystals

LDs developed in HepG2 cells that were exposed to either LDL or oleic acid but were more numerous and larger in cells exposed to both LDL and oleic acid (**Fig. 4**). Only cells exposed to both oleic acid and LDL developed cholesterol crystals within their LDs (Fig. 4). Cholesterol crystallization was noted in the periphery of the LDs adjacent to their membrane (**Fig. 5**), identical to "early" cholesterol crystallization that we observed in vivo in hepatocytes that were not surrounded by KCs in CLS.

Before direct coculture with THP-1 macrophages, HepG2 cells expressed very low levels of *Tnfα*, *Nlrp3*, or *Il1β* mRNA and secreted no IL1b protein into their supernatants, even

TABLE 1. Body and liver weights, hepatic lipid composition, plasma levels, and hepatic histology, after 6 months on high-fat diets supplemented with different concentrations of dietary cholesterol (mean ± SD)

Diet	0% Cholesterol	0.25% Cholesterol	0.5% Cholesterol	0.75% Cholesterol	1% Cholesterol
Body weight (g)	44.5 ± 2.6	47.4 ± 2.9[e]	44.9 ± 4.5	47.5 ± 4.9	46.1 ± 3.2
Body weight gain (%)	60 ± 7	61 ± 5	60 ± 4	70 ± 6	60 ± 8
Liver weight (g)	2.7 ± 0.6	4.0 ± 0.8[d]	4.0 ± 0.9[d]	4.3 ± 1.1[d]	4.5 ± 0.7[d]
Liver weight/body weight (%)	6.0 ± 1.0	8.4 ± 1.3[d]	8.8 ± 1.3[d]	9.0 ± 1.5[d]	9.7 ± 0.9[d]
Food consumption (g/mouse/d)	3.2 ± 0.3	3.3 ± 0.3	3.0 ± 0.3	2.9 ± 0.3[+]	2.9 ± 0.3[+]
Hepatic fat composition (mg/g)					
Triglyceride	383 ± 79	406 ± 75	364 ± 57	336 ± 50	330 ± 34[e]
Cholesterol ester	2.0 ± 0.4	26 ± 20[d]	75 ± 37[d]	120 ± 39[d]	123 ± 42[d]
Free cholesterol	0.68 ± 0.47	0.71 ± 0.56	0.68 ± 0.30	0.69 ± 0.26	0.98 ± 0.61
Free fatty acid	2.70 ± 0.33	2.52 ± 0.42	2.48 ± 0.29	2.15 ± 0.35	2.23 ± 0.27
Epididymal fat composition (mg/g)					
Triglyceride	926 ± 62	878 ± 63	847 ± 74[e]	739 ± 117[d]	717 ± 146[d]
Cholesterol ester	0.12 ± 0.04	0.13 ± 0.06	0.14 ± 0.08	0.16 ± 0.05	0.13 ± 0.06
Free cholesterol	0.28 ± 0.24	0.50 ± 0.32	0.40 ± 0.25	0.60 ± 0.46	0.55 ± 0.41
subcutaneous fat composition (mg/g)					
Triglyceride	857 ± 76	777 ± 110	889 ± 53	877 ± 57	764 ± 152
Cholesterol ester	0.05 ± 0.01	0.04 ± 0.01	0.05 ± 0.02	0.06 ± 0.02	0.05 ± 0.01
Free cholesterol	0.33 ± 0.06	0.35 ± 0.08	0.33 ± 0.07	0.36 ± 0.11	0.37 ± 0.08
Plasma levels (fasting)					
ALT (U/l)	221 ± 55	293 ± 104	304 ± 137	487 ± 104[d]	531 ± 77[d]
Cholesterol (mg/dl)	187 ± 50	269 ± 43[d]	315 ± 73[d]	332 ± 39[d]	338 ± 23[d]
Triglyceride (mg/dl)	55 ± 9	64 ± 8[e]	70 ± 12[d]	70 ± 5[d]	81 ± 29[d]
Glucose (mg/dl)	325 ± 44	321 ± 29	311 ± 23	315 ± 44	324 ± 23
Insulin (ng/ml)	2.7 ± 1.4	5.0 ± 3.3	4.3 ± 4.2	4.5 ± 2.5	4.9 ± 3.3
Hepatic histology					
Steatosis (0–3)[a]	3	3	3	3	3
Lobular inflammation (0–3)[a]	1	1	2	2	2
Fibrosis (0–4)[a]	0	0	1a	1a	1a
Sirius red staining (fibrosis)[b], % area	0.30 ± 0.28	0.27 ± 0.12	1.8 ± 1.4[d]	2.96 ± 2.1[d]	2.24 ± 1.2[d]
Cholesterol crystals[b], % area	0 ± 0	0.29 ± 0.39[e]	7.1 ± 4.32[d]	8.2 ± 4.89[d]	8.5 ± 3.60[d]
Crown-like structures[c], number/field	0.17 ± 0.21	1.24 ± 0.55[e]	7.7 ± 2.2[d]	7.2 ± 2.5[d]	6.6 ± 1.4[d]

Statistical analysis was performed using Student *t* test. Statistically significant difference is compared with the 0% cholesterol group (see footnotes *d* and *e*).

[a]Median values are reported for histological steatosis, inflammation, and fibrosis, scored as follows: steatosis is graded as <5% (0); 5%–33% (1); 34%–66% (2); and >66% (3) of hepatocytes being steatotic at ×200 magnification (28). Lobular inflammation combines mononuclear, fat granulomas and polymorphonuclear leukocytes and is graded as none (0); <2 (1); 2–4 (2); and >4 at ×200 magnification (28). Fibrosis is staged as none (0); perisinusoidal (1a); periportal (1b); periportal and perisinusoidal (2); bridging fibrosis (3); and cirrhosis (4) (28).

[b]Presented as the percentage of the surface area of the liver section that is positive and calculated as the average of 10 random ×200 fields.

[c]Average number of CLSs in 10 random ×200 fields.

[d]$P < 0.01$.

[e]$P < 0.05$.

after exposure to LDL, OA, or LDL + OA for 20 days. Increased expression of *Tnfa*, *Nlrp3*, and *Il1β* mRNA (**Fig. 6A**) and increased secretion of IL1β into the supernatant (Fig. 6B) were demonstrated when PMA-activated THP-1 macrophages were cocultured with cholesterol crystal-containing HepG2 cells (i.e., those previously exposed to LDL + OA) but not when they were cocultured with HepG2 cells without cholesterol crystals (i.e., those previously exposed to LDL alone, OA alone, or control). Direct exposure of THP-1 macrophages to synthetic cholesterol crystals led to profound secretion of IL1β in a dose-dependent manner (Fig. 6C), despite almost no change in *Il1β* mRNA.

When THP-1 cells were added in Transwells® above the HepG2 cells (i.e., "noncontact coculture"), there was no stimulation of THP-1-derived IL-1b, regardless of whether HepG2 cells had been exposed to LDL and oleic acid or not, arguing against the release of a humoral/soluble factor by the HepG2 cells that stimulates the THP-1 cells.

DISCUSSION

We recently reported that cholesterol crystals were present in hepatocyte LDs in experimental and human NASH and that CLSs consisting of activated KCs and macrophages surrounded and processed cholesterol crystal-containing remnant LDs of dead hepatocytes (22). Furthermore, we showed that treatment with ezetimibe and atorvastatin caused resolution of NASH induced by an atherogenic diet in diabetic obese mice, while simultaneously causing dissolution of cholesterol crystals and dispersion of KC-CLSs (27). Here we demonstrate that excess dietary cholesterol is preferentially stored in the liver and that hepatic cholesterol crystals and CLSs develop at the same threshold concentration of dietary cholesterol that also leads to the development of NASH in mice fed a HFHC diet. This suggests a causative association between the development of hepatocyte cholesterol crystals and KC-CLS and the development of NASH. We demonstrate that early

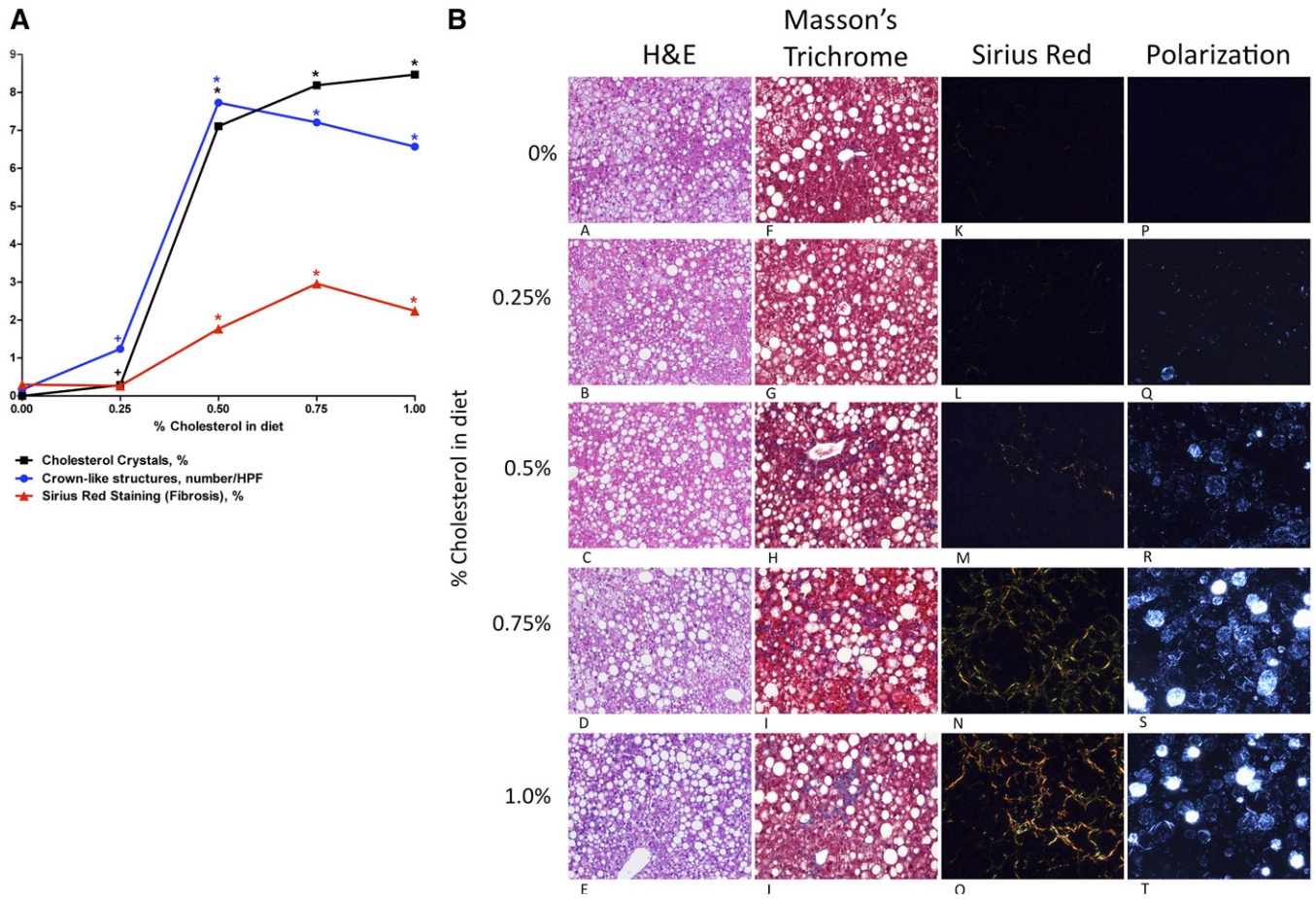

Fig. 1. A: Plot of dietary cholesterol concentration (*x* axis) against hepatic cholesterol crystals (black squares), crown-like structures (blue circles), or Sirius red staining for fibrosis (red triangles), showing the abrupt increase in all three measures that occurs at the same threshold dietary concentration of 0.5%. This suggests that the development of hepatic cholesterol crystals and crown-like structures possibly drives the development of fibrosing NASH. A statistically significant difference in comparison with the 0% cholesterol group is shown. HPF, high-power field. $^{*}P < 0.01$; $^{+}P < 0.05$. B: Mouse liver sections obtained after 6 months on each of the five experimental diets (0%, 0.25%, 0.5%, 0.75%, or 1% dietary cholesterol), all of which contained 15% fat. Sections are stained with H&E, Masson's trichrome, and Sirius red (viewed with polarized light) or are unstained frozen sections viewed with polarized light to look for birefringent cholesterol crystals. Fibrosing steatohepatitis is demonstrated by H&E, Masson's trichrome, and Sirius red at a dietary cholesterol concentration of ⩾0.5%. Also, birefringent cholesterol crystals are seen within hepatocyte LDs at a dietary cholesterol concentration of ⩾0.5% (all at ×200 magnification).

cholesterol crystallization occurs predominantly in the periphery of intact hepatocyte LDs in association with the LD membrane. More intense cholesterol crystallization occurs in the remnant LDs of dead hepatocytes as a result of hydrolysis of cholesterol esters to FC by the lysosomal enzymes of surrounding KCs that form CLSs around them. Exposure of the KCs to cholesterol crystals appears to activate the NLRP3 inflammasome in the KCs, and uptake of FC transforms KCs in CLSs to lipid-laden foam cells. Finally, we describe an in vitro cell culture model of cholesterol crystallization occurring in the periphery of LDs in HepG2 cells induced by LDL and oleic acid in the presence of an ACAT inhibitor that appears identical to the early cholesterol crystallization that we observed in vivo and stimulates NLRP3 activation and IL-1β secretion in cocultured THP-1 macrophages. This suggests that cholesterol crystallization in LDs is indeed initiated in the periphery of the LD in association with the LD membrane and offers an in vitro model for the study of cholesterol crystallization in LDs.

Recent work with artificial membranes suggested that free cholesterol present at high concentration and regular orientation in a membrane can act as a template for cholesterol crystallization to occur adjacent to it (34). Furthermore, models of cholesterol-phospholipid interactions in membranes such as the "umbrella model" predict that after the membrane becomes saturated with cholesterol, any additional cholesterol precipitates to form cholesterol crystals adjacent to the membrane (35). This provides a plausible mechanism for the cholesterol crystallization that we observed in association with LD membranes. We speculate that cholesterol saturation disrupts the function of the LD membrane and the large array of proteins now known to reside on LD membranes by dramatically reducing the fluidity of the LD membrane (21). Cholesterol content is known to critically affect the function of the plasma membrane and of the membranes of intracellular organelles such as the mitochondrial and endoplasmic reticulum by affecting membrane fluidity (36). By analogy the same could be true of the LD

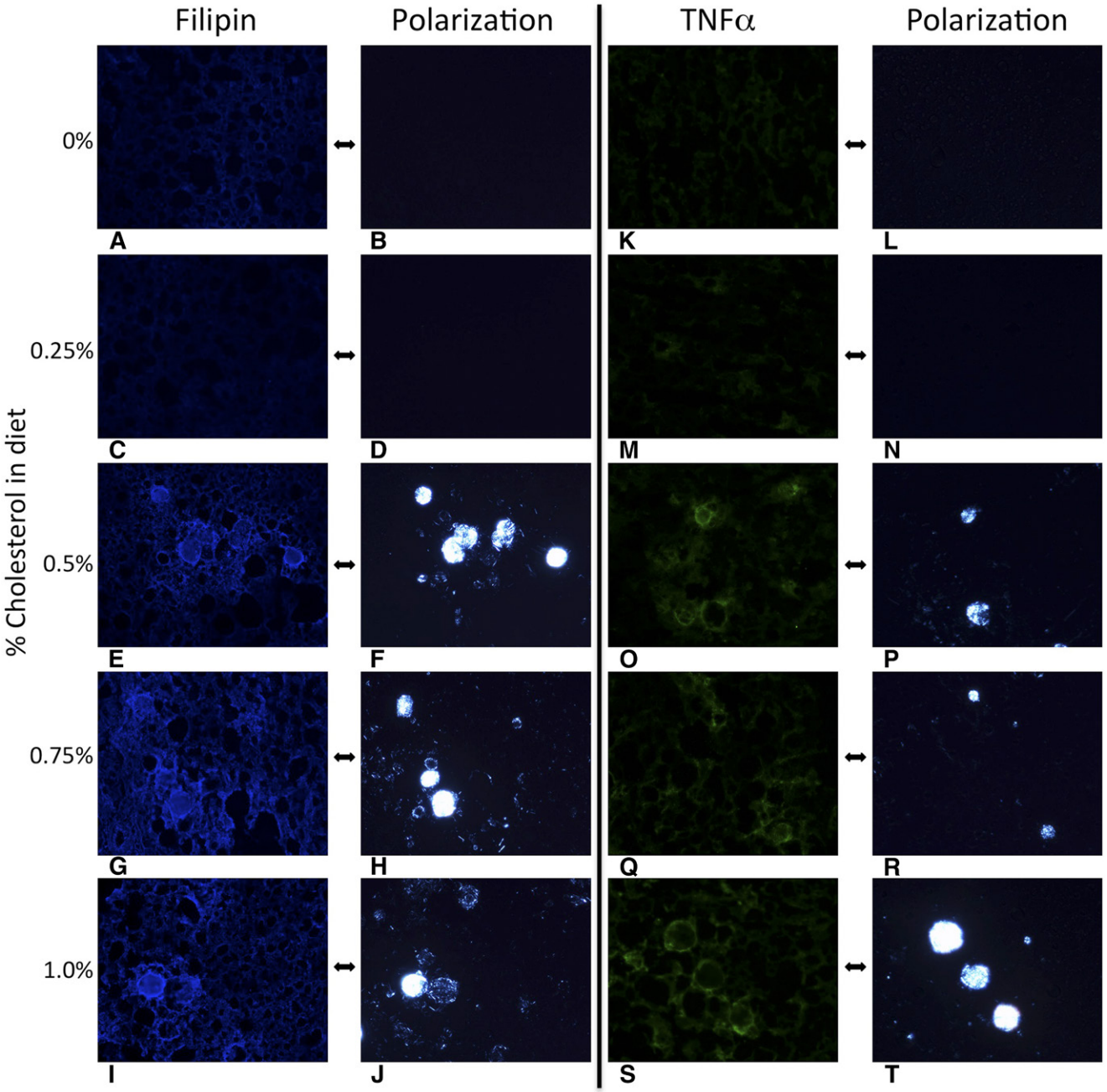

Fig. 2. Hepatocyte cholesterol crystals and Kupffer cell crown-like structures develop at the same threshold of dietary cholesterol that causes fibrosing NASH. Mouse liver sections obtained after 6 months on each of the five experimental diets (0%, 0.25%, 0.5%, 0.75%, or 1% dietary cholesterol), all of which contained 15% fat. Filipin stains free cholesterol blue and demonstrates that the birefringent crystalline material within LDs is indeed cholesterol. TNF-α identifies activated Kupffer cells (green), which are shown to surround LDs with crystalline cholesterol–forming CLSs. Cholesterol crystals and CLSs developed at a threshold cholesterol of dietary concentration of ⩾0.5%, which also caused fibrosing steatohepatitis (all at ×200 magnification).

membrane, although a critical difference is that the LD membrane is a phospholipid monolayer rather than a bilayer. Furthermore, the precipitation of cholesterol crystals adjacent to the LD membrane may also affect the fluidity of the membrane and, in extreme cases of profound crystallization, may even disrupt the physical integrity of the membrane (36). Future experiments will be needed to elucidate the impact of cholesterol crystallization on LD function and to investigate whether it can directly lead to hepatocyte death.

Upon sensing a plethora of structurally diverse pathogen-associated molecular patterns and damage-associated molecular patterns, the NLRP3 inflammasome assembles into a multimolecular platform, which collectively activates caspase-1 by autocatalytic cleavage (37). The active form of caspase-1 then cleaves pro-IL-1β and pro-IL-18 to form biologically active IL-1β and IL-18, which engage innate immune defenses (37) and are important mediators of the inflammatory response. The NLRP3 inflammasome is now thought to drive inflammation in response to exposure to

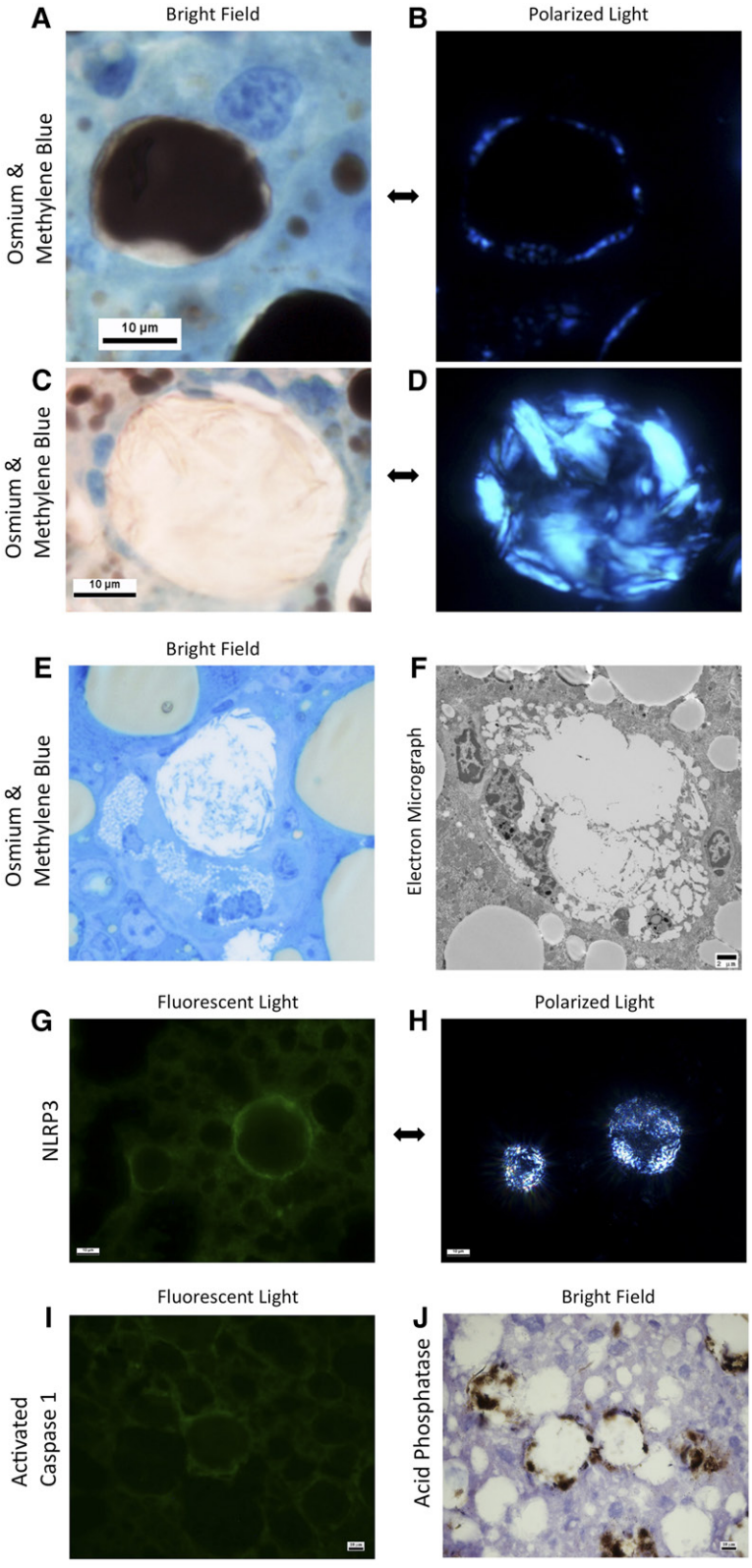

Fig. 3. Mouse liver sections obtained 6 months after a high-cholesterol (1%) and high-fat (15%) diet. Osmium tetroxide staining (stains triglycerides and cholesterol esters black) with methylene blue counterstaining (A–D) shows early cholesterol crystallization under polarized light (B) in the periphery of an intact LD in a normal hepatocyte (A), and advanced cholesterol crystallization (D) with cholesterol crystals as large as 10 μm, in a remnant LD of a dead hepatocyte surrounded by KCs forming a CLS (C). KCs processing remnant LDs of hepatocytes in a CLS transform into characteristic lipid-laden foam cells containing multiple small LDs (E–F). The KCs in CLSs also stain strongly positive for NLRP3 (G) and activated caspase 1 (I) by immunohistochemistry, suggesting activation of the NLRP3 inflammasome. CLSs also stain strongly for acid phosphatase (J), suggesting activation of lysosomal enzymes in the processing of the LD.

crystals that cause human inflammatory conditions such as gout (urate crystals), pseudogout (calcium phosphate dihydrate crystals), silicosis (silica crystals), and asbestosis (asbestos crystals) (38–41). In these conditions, phagocytosis of crystals by macrophages leads to lysosomal swelling and release of cathepsin B, a lysosomal protease, which activates the NLRP3 inflammasome (41). Cholesterol crystals are the latest addition to the group of crystals shown to activate the NLRP3 inflammasome in the macrophages of an important, human chronic inflammatory condition, namely, atherosclerosis (25, 26). Our findings suggest that exposure of KCs to cholesterol crystals within CLSs may activate

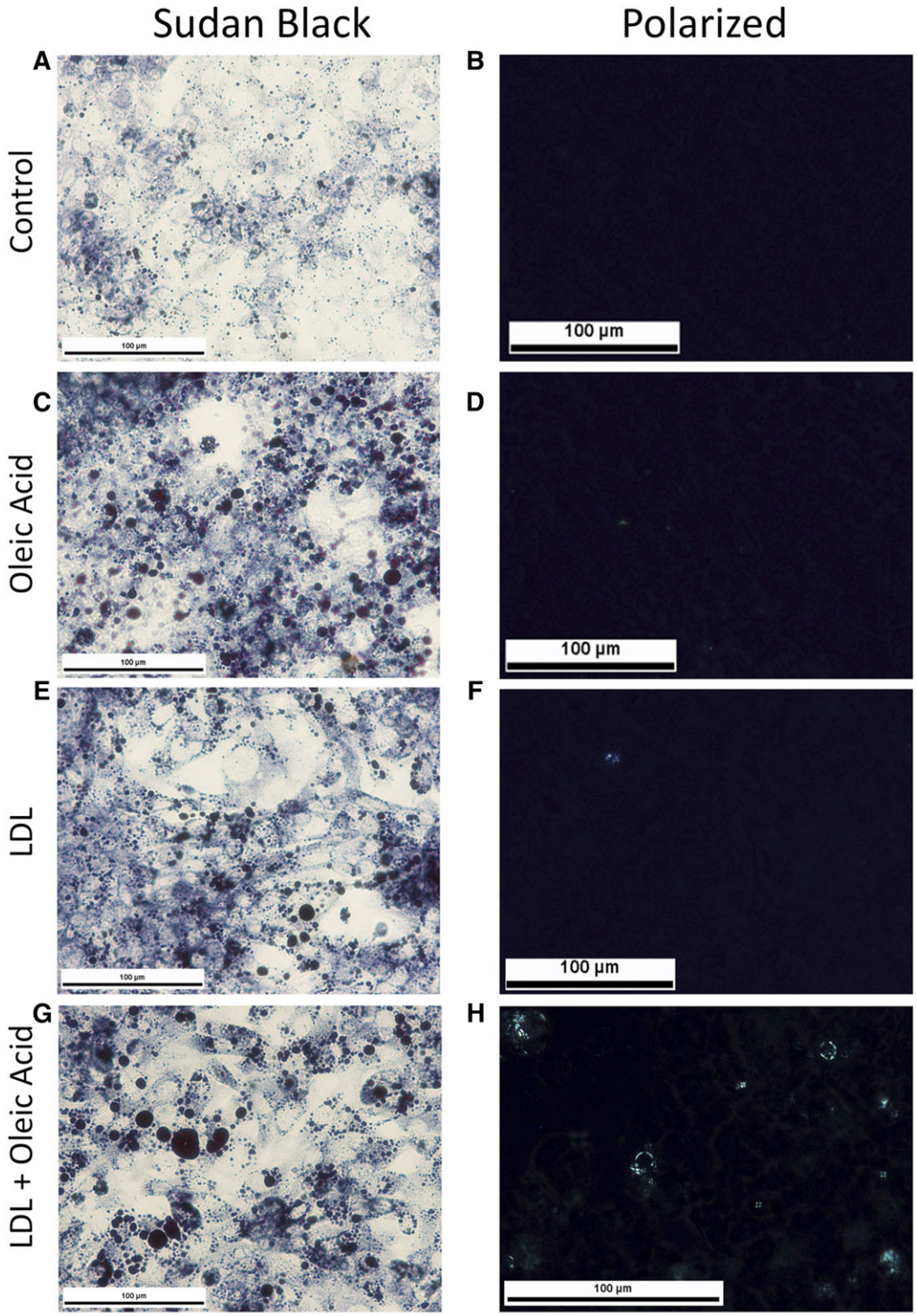

Fig. 4. HepG2 cells exposed to oleic acid and LDL cholesterol develop large lipid droplets that have cholesterol crystals in their periphery, in comparison with control (A, B). Human hepatoma HepG2 cells were plated onto glass chamber slides and exposed to 200 µM of oleic acid (C, D), 2,000 µg/ml of LDL cholesterol (E, F), or both (G, H) for 20 days. Sudan black staining shows large LDs within HepG2 cells with oleic acid (C) or LDL (D), which are even larger with both oleic acid and LDL (G). Under polarized light, only the cells exposed to both oleic acid and LDL had birefringent material consistent with cholesterol crystallization in the periphery of some of the LDs (H).

the NLRP3 inflammasome, leading to chronic inflammation and contributing to the development of NASH.

Our coculture experiments demonstrate that inflammasome activation and production and secretion of IL-1β and TNF-α occurred in activated THP-1 cells (macrophages) exposed to crystals containing HepG2 cells but not in crystals containing HepG2 cells that were not cocultured with THP-1 cells. Thus, even though hepatocytes are in theory

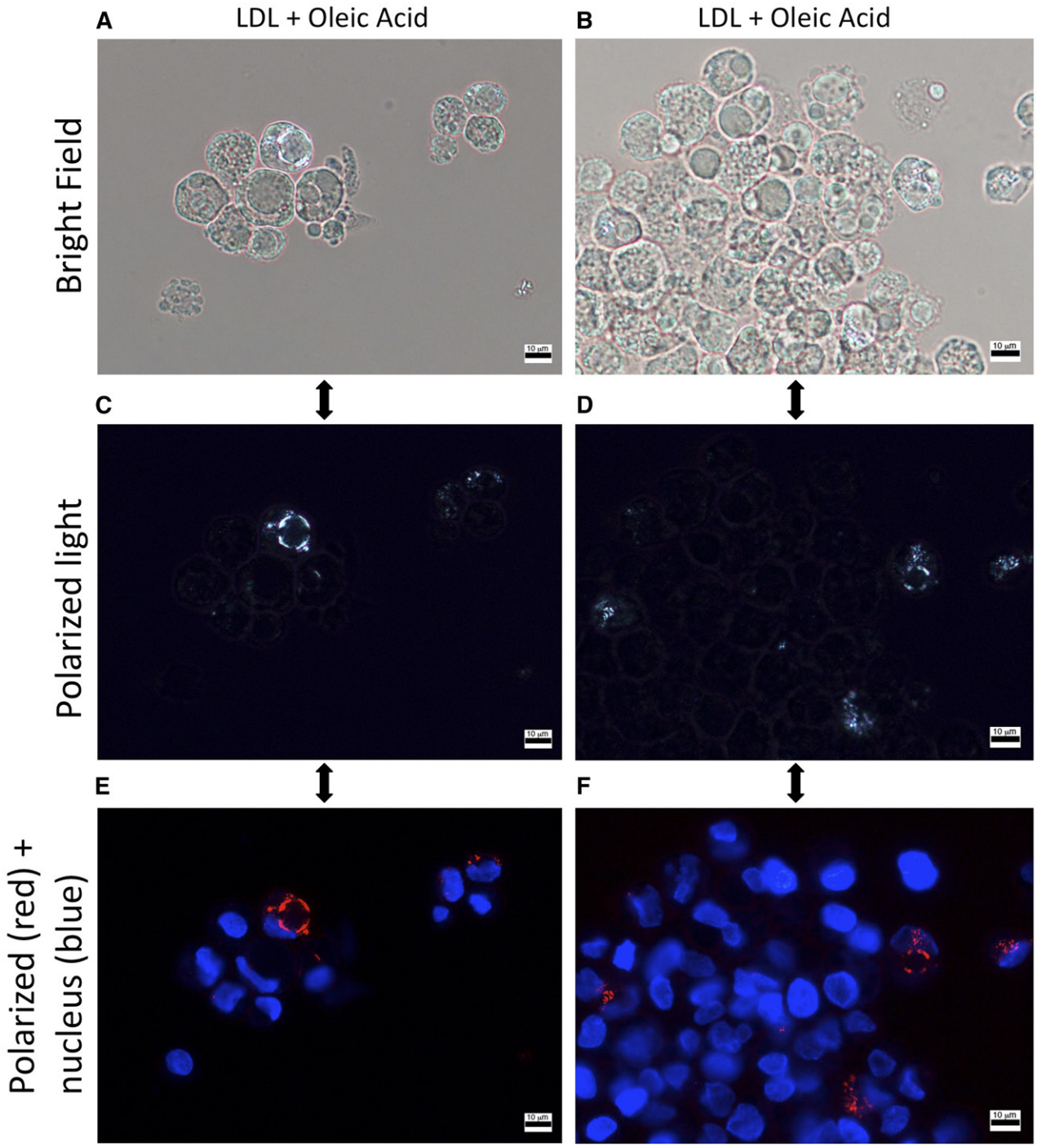

Fig. 5. Cholesterol crystals highlight the membrane of lipid droplets in HepG2 cells exposed to LDL-cholesterol and oleic acid. Human hepatoma HepG2 cells plated onto glass chamber slides and exposed to both 200 µM of oleic acid and 2,000 µg/ml of LDL cholesterol for 20 days. Nuclei are counterstained with Hoescht 33342 (blue). Under polarized light, birefringent material corresponding to cholesterol crystals is seen outlining the periphery of LDs within HepG2 cells. A, C, E: The same slide on which we focused on a single lipid droplet with cholesterol crystallization. B, D, F: Another slide on which we tried to simultaneously show as many lipid droplets as possible (crystals can be in slightly different focal planes within the section).

capable of NLRP3 expression and activation (42, 43), it is macrophages/KCs that have the primary function of secreting inflammatory cytokines when exposed to cholesterol crystals. PMA treatment has been shown to induce pro-IL-1b mRNA in THP-1 cells (26) and therefore acts as the "first signal" in this cell culture model, with subsequent exposure to the cholesterol crystals in the HepG2 cells being the "second signal" that causes NLRP3 activation and cleavage of pro-IL-1b into mature, secreted IL-1b.

It is generally believed that KCs, as with all macrophages, derive most of their cholesterol through receptor-mediated endocytosis of circulating lipoproteins. However, our results suggest a novel mechanism of cholesterol accumulation in hepatic KCs: the processing of hepatocyte

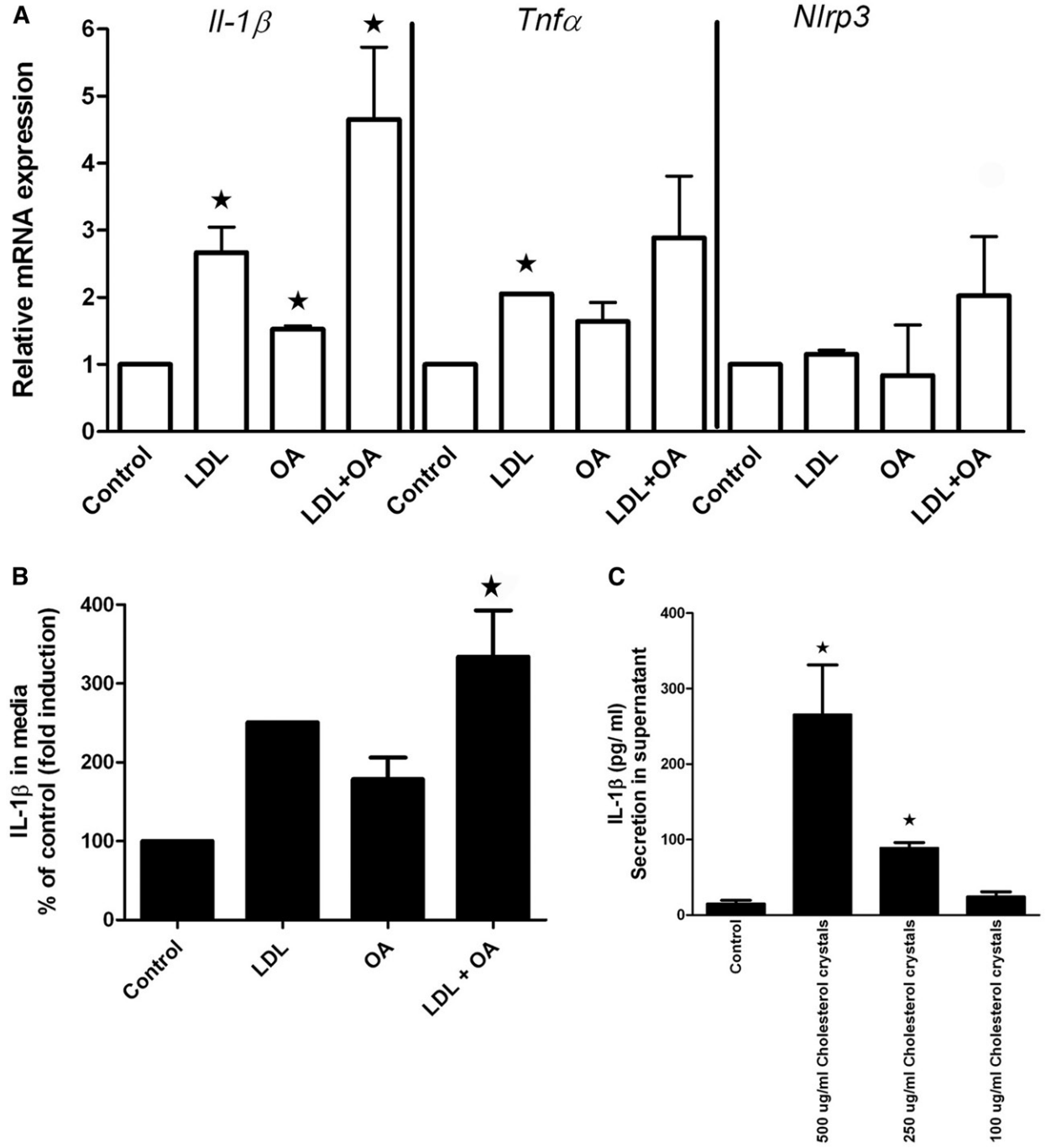

Fig. 6. Induction of IL-1b in THP-1 cells by coculture with cholesterol crystal–containing HepG2 cells or by direct exposure to synthetic cholesterol crystals. A–B: HepG2 cells exposed to 200 μM of oleic acid (OA), 2,000 μg/ml of LDL cholesterol (LDL), or both LDL + OA for 20 days, after which they were cocultured with PMA-activated THP-1 cells (macrophages). A: mRNA expression was measured after 3 h. Increased mRNA expression of Il-1b and to a lesser extent Tnfα and Nlrp3 mRNA by the THP-1 cells was noted when cocultured with HepG2 cells that had been previously exposed to both LDL + OA and had developed cholesterol crystals in their lipid droplets. B: IL-1b in the media at 24 h as measured by ELISA. Results are shown as a percentage of control cells. Significantly increased IL-1b secretion occurred in the THP-1 cells cocultured with HepG2 cells that had been previously exposed to both LDL + OA. C: Exposure of PMA-activated THP-1 cells directly to synthetic cholesterol crystals causes a dose-dependent secretion of IL-1b. ★Results are significant at $P < .05$ in comparison with control.

remnant lipid droplets by lysosomal enzymes of KCs that occurs at the center of CLSs in the extracellular space. This leads to hydrolysis of cholesterol esters (and triglycerides) by lysosomal acid lipase and generation of free cholesterol and cholesterol crystals. Uptake of cholesterol by the KCs in the CLSs causes their transformation into lipid-laden foam cells. This is analogous to the degradation of aggregated LDL by lysosomal enzymes of macrophages in specialized extracellular compartments recently demonstrated in atherosclerosis (44). The main difference is that the digestion

of remnant LDs that we describe by KC-CLSs requires multiple KCs simultaneously forming a tight compartment around the LDs, given the large size of the LDs in relation to the KCs. Future studies will be needed to prove that there is exocytosis of lysosomes by KCs into the remnant LD in the middle of CLSs and acidification of this space required for the enzymatic activity of lysosomal acid lipase.

We found that increasing dietary cholesterol led to cholesterol loading of the liver but not of adipose tissue. Excess dietary cholesterol was stored almost exclusively in the liver within hepatocyte lipid droplets after conversion into cholesterol ester rather than in adipose tissue. We found limited confirmatory literature on this potentially important topic (45). Our findings are consistent with the extensive dysregulation of hepatic cholesterol homeostasis that has been documented in NAFLD, leading to increased hepatic cholesterol levels (46, 47) and ultimately resulting in crystallization of cholesterol in hepatocyte lipid droplets. We found no cholesterol crystals in adipocyte lipid droplets, consistent with the low concentration of cholesterol in adipose tissue (data not shown).

A schematic representation of our hypothesized mechanism of hepatic cholesterol crystal-induced NASH is shown in **Fig. 7**. First, in the setting of hepatic cholesterol loading, cholesterol crystallization occurs initially in hepatocytes in the periphery of large LDs in close association with the LD membrane, likely as a result of high free-cholesterol concentration on the LD membrane. Cholesterol crystallization likely disrupts LD membrane function, because all cellular membranes are exquisitely sensitive to cholesterol content, but does not appear to activate the NLRP3 inflammasome in hepatocytes based on our cell culture findings.

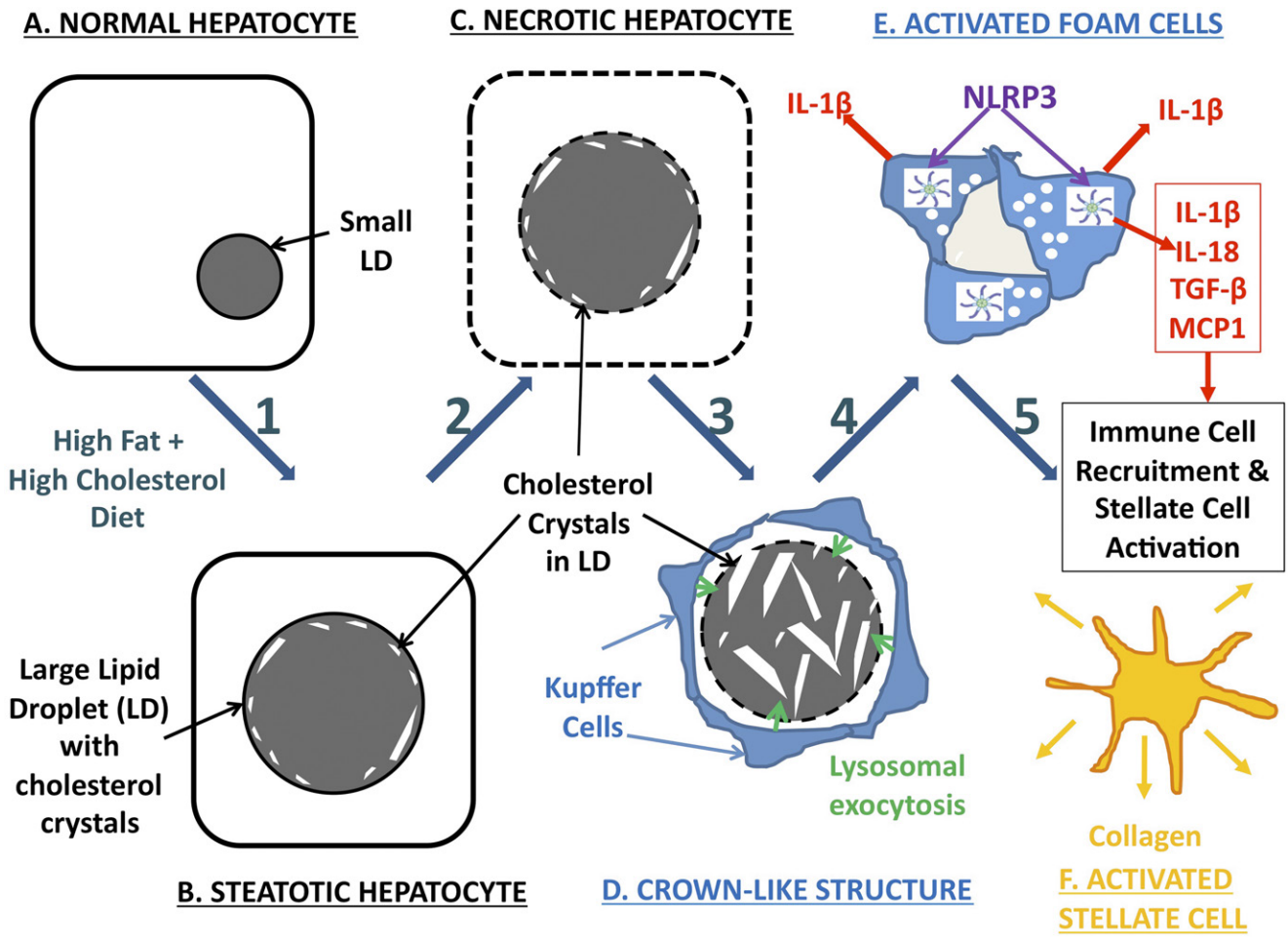

Fig. 7. Schematic representation of our hypothesized mechanism of hepatic cholesterol crystal–induced NASH, involving the following components: Steps 1–2: As a result of a HFHC diet (A) or other causes of hepatic cholesterol loading, large lipid droplets form within hepatocytes (B), and cholesterol crystallization occurs (C) initially in the periphery of large LDs in close association with the LD membrane, likely as a result of precipitation of supersaturated cholesterol from the LD membrane. Cholesterol crystallization disrupts LD membrane function. Step 3: KCs aggregate around necrotic hepatocytes containing cholesterol crystals in response to the chemotactic signals produced by the hepatocytes, forming CLSs. KCs in the CLS hydrolyze the remnant LDs of dead hepatocytes in the extracellular space, possibly by lysosomal exocytosis (D), and additional cholesterol crystals are formed because of the hydrolysis of cholesterol esters into FC by lysosomal acid lipase. Step 4: Uptake of this FC by KCs and exposure to cholesterol crystals transform KCs into activated lipid-laden foam cells (E). Exposure of KCs to cholesterol crystals causes activation of the NLRP3 inflammasome within KCs, which leads to production of proinflammatory cytokines and chemokines by KCs and propagates the chronic "sterile" inflammation of NASH. Step 5: Chemotactic signals produced by crystal-activated KCs attract an inflammatory infiltrate of additional KCs and neutrophils, as well as causing aggregation, activation, and transformation of stellate cells into collagen-producing myofibroblasts (F), leading to fibrosing NASH and, ultimately, cirrhosis.

Second, KCs aggregate around dead hepatocytes containing cholesterol crystals forming CLSs. KCs in the CLS hydrolyze the remnant LDs of dead hepatocytes in the extracellular space, possibly by lysosomal exocytosis, and additional cholesterol crystals are formed because of the hydrolysis of cholesterol esters into FC by lysosomal acid lipase. Third, KCs exposed to cholesterol crystals transform into activated, lipid-laden foam cells. Exposure of KCs to cholesterol crystals causes activation of the NLRP3 inflammasome within KCs, which leads to production of proinflammatory cytokines and chemokines by KCs and propagates the chronic "sterile" inflammation of NASH. Finally, chemotactic signals produced by crystal-activated KCs attract an inflammatory infiltrate of additional KCs and neutrophils, as well as causing aggregation, activation, and transformation of stellate cells into collagen-producing myofibroblasts, leading to fibrosing NASH and, ultimately, cirrhosis.

This mechanistic hypothesis has therapeutic implications for human NASH. Cholesterol-lowering drugs are widely available and, as we have recently shown, can reverse hepatic cholesterol crystallization and simultaneously reverse experimental fibrosing NASH (27). Recently a novel, first-in-class, oral, specific NLRP3 inhibitor has been described (48, 49); therefore, pharmacological NLRP3 inhibition could also be a potential therapeutic approach in NASH if our hypotheses are proven correct.

REFERENCES

1. Matteoni, C. A., Z. M. Younossi, T. Gramlich, N. Boparai, Y. C. Liu, and A. J. McCullough. 1999. Nonalcoholic fatty liver disease: a spectrum of clinical and pathological severity. *Gastroenterology.* **116:** 1413–1419.
2. Bugianesi, E., N. Leone, E. Vanni, G. Marchesini, F. Brunello, P. Carucci, A. Musso, P. De Paolis, L. Capussotti, M. Salizzoni, et al. 2002. Expanding the natural history of nonalcoholic steatohepatitis: from cryptogenic cirrhosis to hepatocellular carcinoma. *Gastroenterology.* **123:** 134–140.
3. Matsuzawa, N., T. Takamura, S. Kurita, H. Misu, T. Ota, H. Ando, M. Yokoyama, M. Honda, Y. Zen, Y. Nakanuma, et al. 2007. Lipid-induced oxidative stress causes steatohepatitis in mice fed an atherogenic diet. *Hepatology.* **46:** 1392–1403.
4. Zheng, S., L. Hoos, J. Cook, G. Tetzloff, H. Davis, Jr., M. van Heek, and J. J. Hwa. 2008. Ezetimibe improves high fat and cholesterol diet-induced non-alcoholic fatty liver disease in mice. *Eur. J. Pharmacol.* **584:** 118–124.
5. Van Rooyen, D. M., C. Z. Larter, W. G. Haigh, M. M. Yeh, G. Ioannou, R. Kuver, S. P. Lee, N. C. Teoh, and G. C. Farrell. 2011. Hepatic free cholesterol accumulates in obese, diabetic mice and causes nonalcoholic steatohepatitis. *Gastroenterology.* **141:** 1393–1403, 1403.e1–5.
6. Savard, C., E. V. Tartaglione, R. Kuver, W. G. Haigh, G. C. Farrell, S. Subramanian, A. Chait, M. M. Yeh, L. S. Quinn, and G. N. Ioannou. 2013. Synergistic interaction of dietary cholesterol and dietary fat in inducing experimental steatohepatitis. *Hepatology.* **57:** 81–92.
7. Van Rooyen, D. M., L. T. Gan, M. M. Yeh, W. G. Haigh, C. Z. Larter, G. Ioannou, N. C. Teoh, and G. C. Farrell. 2013. Pharmacological cholesterol lowering reverses fibrotic NASH in obese, diabetic mice with metabolic syndrome. *J. Hepatol.* **59:** 144–152.
8. Puri, P., R. A. Baillie, M. M. Wiest, F. Mirshahi, J. Choudhury, O. Cheung, C. Sargeant, M. J. Contos, and A. J. Sanyal. 2007. A lipidomic analysis of nonalcoholic fatty liver disease. *Hepatology.* **46:** 1081–1090.
9. Wouters, K., M. van Bilsen, P. J. van Gorp, V. Bieghs, D. Lutjohann, A. Kerksiek, B. Staels, M. H. Hofker, and R. Shiri-Sverdlov. 2010. Intrahepatic cholesterol influences progression, inhibition and reversal of non-alcoholic steatohepatitis in hyperlipidemic mice. *FEBS Lett.* **584:** 1001–1005.
10. Wouters, K., P. J. van Gorp, V. Bieghs, M. J. Gijbels, H. Duimel, D. Lutjohann, A. Kerksiek, R. van Kruchten, N. Maeda, B. Staels, et al. 2008. Dietary cholesterol, rather than liver steatosis, leads to hepatic inflammation in hyperlipidemic mouse models of nonalcoholic steatohepatitis. *Hepatology.* **48:** 474–486.
11. Bieghs, V., P. J. Van Gorp, K. Wouters, T. Hendrikx, M. J. Gijbels, M. van Bilsen, J. Bakker, C. J. Binder, D. Lutjohann, B. Staels, et al. 2012. LDL receptor knock-out mice are a physiological model particularly vulnerable to study the onset of inflammation in non-alcoholic fatty liver disease. *PLoS One.* **7:** e30668.
12. Subramanian, S., L. Goodspeed, S. Wang, J. Kim, L. Zeng, G. N. Ioannou, W. G. Haigh, M. M. Yeh, K. V. Kowdley, K. D. O'Brien, et al. 2011. Dietary cholesterol exacerbates hepatic steatosis and inflammation in obese LDL receptor-deficient mice. *J. Lipid Res.* **52:** 1626–1635.
13. Ioannou, G. N., O. B. Morrow, M. L. Connole, and S. P. Lee. 2009. Association between dietary nutrient composition and the incidence of cirrhosis or liver cancer in the United States population. *Hepatology.* **50:** 175–184.
14. Yoneda, M., K. Fujita, Y. Nozaki, H. Endo, H. Takahashi, K. Hosono, K. Suzuki, H. Mawatari, H. Kirikoshi, M. Inamori, et al. 2010. Efficacy of ezetimibe for the treatment of non-alcoholic steatohepatitis: an open-label, pilot study. *Hepatol. Res.* **40:** 566–573.
15. Park, H., T. Shima, K. Yamaguchi, H. Mitsuyoshi, M. Minami, K. Yasui, Y. Itoh, T. Yoshikawa, M. Fukui, G. Hasegawa, et al. 2011. Efficacy of long-term ezetimibe therapy in patients with nonalcoholic fatty liver disease. *J. Gastroenterol.* **46:** 101–107.
16. Athyros, V. G., K. Tziomalos, T. D. Gossios, T. Griva, P. Anagnostis, K. Kargiotis, E. D. Pagourelias, E. Theocharidou, A. Karagiannis, D. P. Mikhailidis, et al. 2010. Safety and efficacy of long-term statin treatment for cardiovascular events in patients with coronary heart disease and abnormal liver tests in the Greek Atorvastatin and Coronary Heart Disease Evaluation (GREACE) Study: a post-hoc analysis. *Lancet.* **376:** 1916–1922.
17. Athyros, V. G., D. P. Mikhailidis, T. P. Didangelos, O. I. Giouleme, E. N. Liberopoulos, A. Karagiannis, A. I. Kakafika, K. Tziomalos, A. K. Burroughs, and M. S. Elisaf. 2006. Effect of multifactorial treatment on non-alcoholic fatty liver disease in metabolic syndrome: a randomised study. *Curr. Med. Res. Opin.* **22:** 873–883.
18. Foster, T., M. J. Budoff, S. Saab, N. Ahmadi, C. Gordon, and A. D. Guerci. 2011. Atorvastatin and antioxidants for the treatment of nonalcoholic fatty liver disease: the St Francis Heart Study randomized clinical trial. *Am. J. Gastroenterol.* **106:** 71–77.
19. Nelson, A., D. M. Torres, A. E. Morgan, C. Fincke, and S. A. Harrison. 2009. A pilot study using simvastatin in the treatment of nonalcoholic steatohepatitis: a randomized placebo-controlled trial. *J. Clin. Gastroenterol.* **43:** 990–994.
20. Chan, D. C., G. F. Watts, S. K. Gan, E. M. Ooi, and P. H. Barrett. 2010. Effect of ezetimibe on hepatic fat, inflammatory markers, and apolipoprotein B-100 kinetics in insulin-resistant obese subjects on a weight loss diet. *Diabetes Care.* **33:** 1134–1139.
21. Ioannou, G. N. 2016. The role of cholesterol in the pathogenesis of NASH. *Trends Endocrinol. Metab.* **27:** 84–95.
22. Ioannou, G. N., W. G. Haigh, D. Thorning, and C. Savard. 2013. Hepatic cholesterol crystals and crown-like structures distinguish NASH from simple steatosis. *J. Lipid Res.* **54:** 1326–1334.
23. Cinti, S., G. Mitchell, G. Barbatelli, I. Murano, E. Ceresi, E. Faloia, S. Wang, M. Fortier, A. S. Greenberg, and M. S. Obin. 2005. Adipocyte death defines macrophage localization and function in adipose tissue of obese mice and humans. *J. Lipid Res.* **46:** 2347–2355.
24. Strissel, K. J., Z. Stancheva, H. Miyoshi, J. W. Perfield II, J. DeFuria, Z. Jick, A. S. Greenberg, and M. S. Obin. 2007. Adipocyte death, adipose tissue remodeling, and obesity complications. *Diabetes.* **56:** 2910–2918.
25. Duewell, P., H. Kono, K. J. Rayner, C. M. Sirois, G. Vladimer, F. G. Bauernfeind, G. S. Abela, L. Franchi, G. Nunez, M. Schnurr, et al. 2010. NLRP3 inflammasomes are required for atherogenesis and activated by cholesterol crystals. *Nature.* **464:** 1357–1361.
26. Rajamäki, K., J. Lappalainen, K. Oorni, E. Valimaki, S. Matikainen, P. T. Kovanen, and K. K. Eklund. 2010. Cholesterol crystals activate the NLRP3 inflammasome in human macrophages: a novel link between cholesterol metabolism and inflammation. *PLoS One.* **5:** e11765.
27. Ioannou, G. N., D. M. Van Rooyen, C. Savard, W. G. Haigh, M. M. Yeh, N. C. Teoh, and G. C. Farrell. 2015. Cholesterol-lowering drugs

cause dissolution of cholesterol crystals and disperse Kupffer cell crown-like structures during resolution of NASH. *J. Lipid Res.* **56:** 277–285.
28. Kleiner, D. E., E. M. Brunt, M. Van Natta, C. Behling, M. J. Contos, O. W. Cummings, L. D. Ferrell, Y. C. Liu, M. S. Torbenson, A. Unalp-Arida, et al. 2005. Design and validation of a histological scoring system for nonalcoholic fatty liver disease. *Hepatology.* **41:** 1313–1321.
29. Rudolf, M., and C. A. Curcio. 2009. Esterified cholesterol is highly localized to Bruch's membrane, as revealed by lipid histochemistry in wholemounts of human choroid. *J. Histochem. Cytochem.* **57:** 731–739.
30. Ganz, M., T. Csak, B. Nath, and G. Szabo. 2011. Lipopolysaccharide induces and activates the Nalp3 inflammasome in the liver. *World J. Gastroenterol.* **17:** 4772–4778.
31. Folch, J., M. Lees, and G. H. Sloane Stanley. 1957. A simple method for the isolation and purification of total lipides from animal tissues. *J. Biol. Chem.* **226:** 497–509.
32. Negash, A. A., H. J. Ramos, N. Crochet, D. T. Lau, B. Doehle, N. Papic, D. A. Delker, J. Jo, A. Bertoletti, C. H. Hagedorn, et al. 2013. IL-1beta production through the NLRP3 inflammasome by hepatic macrophages links hepatitis C virus infection with liver inflammation and disease. *PLoS Pathog.* **9:** e1003330.
33. Horner, S. M., H. M. Liu, H. S. Park, J. Briley, and M. Gale, Jr. 2011. Mitochondrial-associated endoplasmic reticulum membranes (MAM) form innate immune synapses and are targeted by hepatitis C virus. *Proc. Natl. Acad. Sci. USA.* **108:** 14590–14595.
34. Varsano, N., I. Fargion, S. G. Wolf, L. Leiserowitz, and L. Addadi. 2015. Formation of 3D cholesterol crystals from 2D nucleation sites in lipid bilayer membranes: implications for atherosclerosis. *J. Am. Chem. Soc.* **137:** 1601–1607.
35. Huang, J., and G. W. Feigenson. 1999. A microscopic interaction model of maximum solubility of cholesterol in lipid bilayers. *Biophys. J.* **76:** 2142–2157.
36. Tabas, I. 2002. Consequences of cellular cholesterol accumulation: basic concepts and physiological implications. *J. Clin. Invest.* **110:** 905–911.
37. Schroder, K., and J. Tschopp. 2010. The inflammasomes. *Cell.* **140:** 821–832.
38. Martinon, F., V. Petrilli, A. Mayor, A. Tardivel, and J. Tschopp. 2006. Gout-associated uric acid crystals activate the NALP3 inflammasome. *Nature.* **440:** 237–241.
39. Hornung, V., F. Bauernfeind, A. Halle, E. O. Samstad, H. Kono, K. L. Rock, K. A. Fitzgerald, and E. Latz. 2008. Silica crystals and aluminum salts activate the NALP3 inflammasome through phagosomal destabilization. *Nat. Immunol.* **9:** 847–856.
40. Dostert, C., V. Petrilli, R. Van Bruggen, C. Steele, B. T. Mossman, and J. Tschopp. 2008. Innate immune activation through Nalp3 inflammasome sensing of asbestos and silica. *Science.* **320:** 674–677.
41. Cassel, S. L., S. C. Eisenbarth, S. S. Iyer, J. J. Sadler, O. R. Colegio, L. A. Tephly, A. B. Carter, P. B. Rothman, R. A. Flavell, and F. S. Sutterwala. 2008. The Nalp3 inflammasome is essential for the development of silicosis. *Proc. Natl. Acad. Sci. USA.* **105:** 9035–9040.
42. Wree, A., A. Eguchi, M. D. McGeough, C. A. Pena, C. D. Johnson, A. Canbay, H. M. Hoffman, and A. E. Feldstein. 2014. NLRP3 inflammasome activation results in hepatocyte pyroptosis, liver inflammation, and fibrosis in mice. *Hepatology.* **59:** 898–910.
43. Miao, E. A., J. V. Rajan, and A. Aderem. 2011. Caspase-1-induced pyroptotic cell death. *Immunol. Rev.* **243:** 206–214.
44. Haka, A. S., I. Grosheva, E. Chiang, A. R. Buxbaum, B. A. Baird, L. M. Pierini, and F. R. Maxfield. 2009. Macrophages create an acidic extracellular hydrolytic compartment to digest aggregated lipoproteins. *Mol. Biol. Cell.* **20:** 4932–4940.
45. Wiggers, K. D., M. J. Richard, J. W. Stewart, N. L. Jacobson, and P. J. Berger. 1977. Type and amount of dietary fat affect relative concentration of cholesterol in blood and other tissues of rats. *Atherosclerosis.* **27:** 27–34.
46. Musso, G., R. Gambino, and M. Cassader. 2013. Cholesterol metabolism and the pathogenesis of non-alcoholic steatohepatitis. *Prog. Lipid Res.* **52:** 175–191.
47. Min, H. K., A. Kapoor, M. Fuchs, F. Mirshahi, H. Zhou, J. Maher, J. Kellum, R. Warnick, M. J. Contos, and A. J. Sanyal. 2012. Increased hepatic synthesis and dysregulation of cholesterol metabolism is associated with the severity of nonalcoholic fatty liver disease. *Cell Metab.* **15:** 665–674.
48. Coll, R. C., A. A. Robertson, J. J. Chae, S. C. Higgins, R. Munoz-Planillo, M. C. Inserra, I. Vetter, L. S. Dungan, B. G. Monks, A. Stutz, et al. 2015. A small-molecule inhibitor of the NLRP3 inflammasome for the treatment of inflammatory diseases. *Nat. Med.* **21:** 248–255.
49. Mridha, A. R., A. Wree, A. A. Robertson, M. M. Yeh, C. D. Johnson, D. M. Van Rooyen, F. Haczeyni, N. C. Teoh, C. Savard, G. N. Ioannou, et al. 2017. NLRP3 inflammasome blockade reduces liver inflammation and fibrosis in experimental NASH in mice. *J. Hepatol.* **66:** 1037–1046.